

Structure-Based Design and Synthesis of Novel Inhibitors Targeting HDAC8 from *Schistosoma mansoni* for the Treatment of Schistosomiasis

Tino Heimburg,^{†,‡} Alokta Chakrabarti,^{‡,‡} Julien Lancelot,[§] Martin Marek,^{||} Jelena Melesina,[†] Alexander-Thomas Hauser,[‡] Tajith B. Shaik,^{||} Sylvie Duclaud,^{||} Dina Robaa,[†] Frank Erdmann,[†] Matthias Schmidt,[†] Christophe Romier,^{||} Raymond J. Pierce,[§] Manfred Jung,[‡] and Wolfgang Sippl^{*,†}

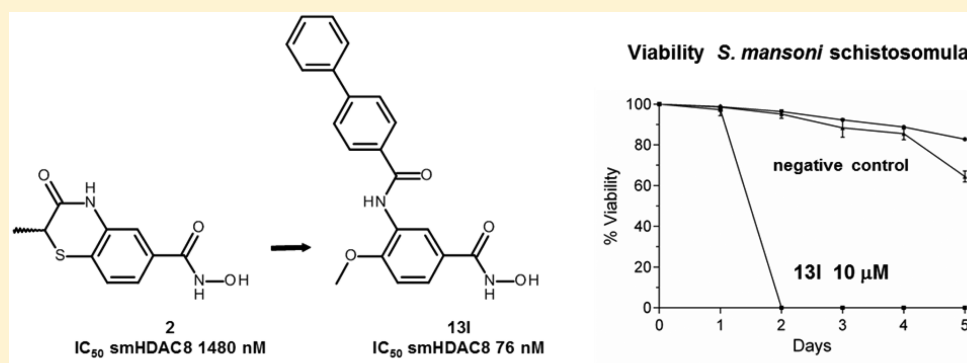
[†]Institute of Pharmacy, Martin-Luther University of Halle-Wittenberg, 06120 Halle/Saale, Germany

[‡]Institute of Pharmaceutical Sciences, University of Freiburg, 79104 Freiburg, Germany

[§]Université de Lille, CNRS, Inserm, CHU Lille, Institut Pasteur de Lille, U1019 - UMR 8204 - CIIL - Centre d'Infection et d'Immunité de Lille, 59000 Lille, France

^{||}Département de Biologie Structurale Intégrative, Institut de Génétique et Biologie Moléculaire et Cellulaire (IGBMC), Université de Strasbourg (UDS), CNRS, INSERM, 67404 Illkirch Cedex, France

Supporting Information



ABSTRACT: Schistosomiasis is a major neglected parasitic disease that affects more than 265 million people worldwide and for which the control strategy consists of mass treatment with the only available drug, praziquantel. In this study, a series of new benzohydroxamates were prepared as potent inhibitors of *Schistosoma mansoni* histone deacetylase 8 (smHDAC8). Crystallographic analysis provided insights into the inhibition mode of smHDAC8 activity by these 3-amidobenzohydroxamates. The newly designed inhibitors were evaluated in screens for enzyme inhibitory activity against schistosome and human HDACs. Twenty-seven compounds were found to be active in the nanomolar range, and some of them showed selectivity toward smHDAC8 over the major human HDACs (1 and 6). The active benzohydroxamates were additionally screened for lethality against the schistosome larval stage using a fluorescence-based assay. Four of these showed significant dose-dependent killing of the schistosome larvae and markedly impaired egg laying of adult worm pairs maintained in culture.

INTRODUCTION

Schistosomiasis is one of the major neglected parasitic diseases,¹ second in importance only to malaria. It is caused by parasites from the genus *Schistosoma*,^{2,3} with *Schistosoma mansoni* being the most widely distributed species.⁴ Worldwide more than 265 million individuals are infected,⁵ of whom 280 000 die annually.^{4,6} To date there is no effective vaccine available, and control depends on mass drug administration using the only available treatment, praziquantel, which is effective against all species of human schistosomiasis.^{7,8} In 2013 over 30 million people were treated in sub-Saharan Africa,⁹ and this raises serious concerns about the selection of drug resistance. The reduced efficiency of praziquantel and the

observed resistance in laboratory strains underline the need to consider alternative therapeutic strategies.^{7,8,10,11} Indeed, drug resistance represents an increasing problem for the treatment of a number of parasitic diseases for which only a few drugs are available. Thus, novel potential drug targets and drug candidates against eukaryotic parasites are urgently required.¹²

Histone modifying enzymes (HMEs), which are responsible for post-translational modifications of histone and non-histone substrates, have been reported as drug targets for many diseases such as cancer, inflammation, metabolic diseases, and neuro-

Received: September 23, 2015

Published: March 3, 2016

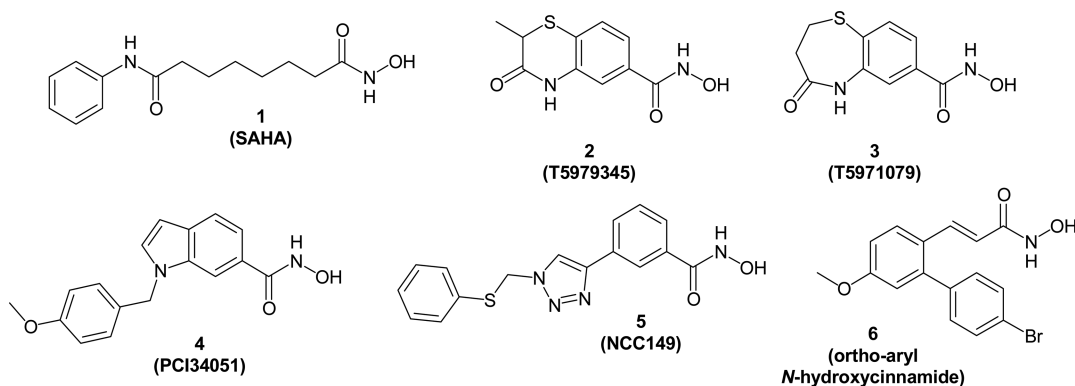


Figure 1. Chemical structures of pan-HDAC inhibitor **1** (SAHA) and reported hHDAC8 inhibitors.

psychiatric disorders as well as in regenerative medicine.^{13–16} One of the best-investigated post-translational modifications is acetylation/deacetylation of lysine residues in histone and non-histone proteins. The processes of acetylation and deacetylation are controlled by histone acetyl transferases (HATs) and histone deacetylases (HDACs), respectively. The equilibrium between acetylated and non-acetylated histone proteins must be maintained for proper transcriptional activity and cellular function.¹⁷ Additionally, an increasing number of non-histone proteins have been reported as substrates of HDACs.¹⁸ These proteins may be involved in transcription complexes, which play a pivotal role in the regulation of gene expression as well as cell proliferation, migration, death, and angiogenesis.¹⁸ HDACs are a family of enzymes found in many organisms, including bacteria, fungi, plants, and animals. Eighteen different members of the HDAC family have been annotated in the human genome and have been classified into four categories on the basis of their homology to yeast HDACs.¹⁹ Class I consists of four different subtypes (HDAC1, -2, -3, and -8) and shows homology to the yeast protein RPD3. Class II includes six subtypes, which are divided into two subclasses: class IIa with subtypes HDAC4, -5, -7, and -9 and class IIb with HDAC6 and -10. HDAC11 is placed in class IV. While the activity of the enzymes belonging to class I, II, and IV HDACs depends on a zinc-based catalytic mechanism, class III enzymes, also called sirtuins, use nicotinamide adenine dinucleotide as a cofactor.²⁰ Hereafter, the term HDAC will refer only to the classical zinc-dependent deacetylases.

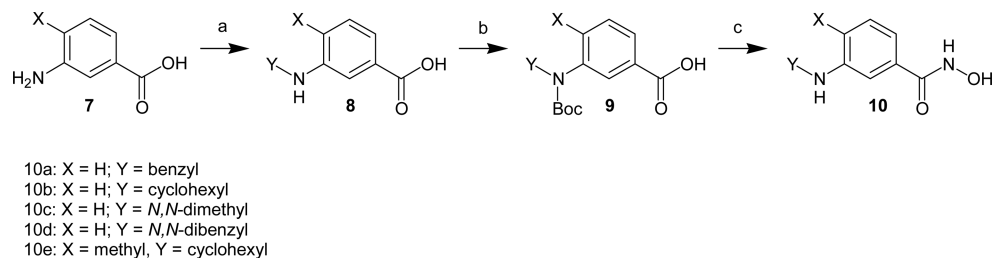
Numerous HDAC inhibitors (HDACi) have been identified in the past decade; several are in clinical trials, and five are currently approved for the treatment of cancer, for example, the aliphatic hydroxamate SAHA (**1**) (Figure 1), marketed under the name Vorinostat.^{21–26} The pan-inhibitor **1** is a weak inhibitor of HDAC8 (μM range). Several aromatic^{27–29} and cinnamic acid-based³⁰ hydroxamates have recently been developed as selective inhibitors of human HDAC8 (**2–6**; Figure 1). The indole derivative **4**²⁷ is the most selective HDAC8 inhibitor in vitro, with an IC_{50} of 10 nM for HDAC8 and selectivity indexes of 290 and 400 for HDAC8 over HDAC6 and HDAC1, respectively. Recent investigations^{14,15,31,32} have shown that eukaryotic parasites possess HDAC orthologues and that histone acetylation seems to play a key role in gene-transcription regulation and cell-cycle progression. Also, many human parasites share several characteristics with tumor cells, including high metabolic activity, a dependence on lactate fermentation as an energy source within the human host, uncontrolled cell division, and a

degree of invisibility to the host immune responses.¹⁴ The therapeutic potential of HDAC inhibitors as antiparasitic agents was first shown for the cyclic tetrapeptide apicidin.³¹ In addition, several studies using various HDACi demonstrated the antiproliferative and antiparasitic activities of these inhibitors on major human parasitic diseases such as leishmaniasis, malaria, schistosomiasis, toxoplasmosis, and trypanosomiasis.^{14,15}

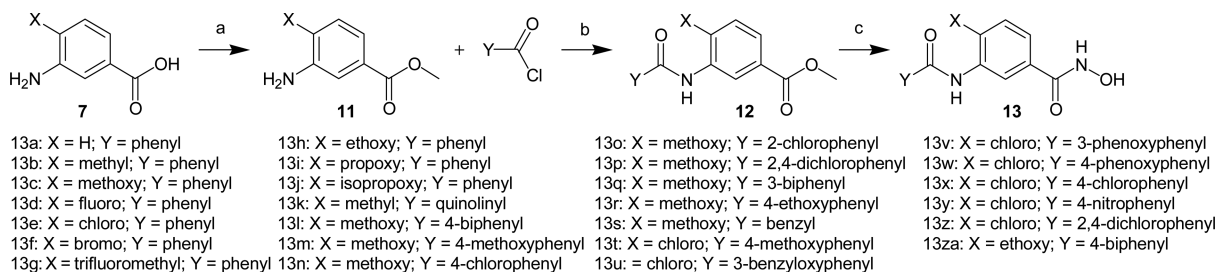
To date, only class I (smHDAC1, -3, and -8) and class III (smSirt1, -2, -5, -6, and -7) HDACs of *S. mansoni* have been cloned and characterized.^{33,34} Treatment of schistosomes with generic HDAC inhibitors caused protein acetylation and dose-dependent mortality of schistosome larvae (schistosomula) and adult worms.³³ All three *S. mansoni* class I HDACs (smHDAC1, -3, and -8) are expressed at all life-cycle stages, with HDAC8 transcripts always being the most abundant,³² indicating that this latter enzyme is a potential target for the design of schistosome-specific inhibitors. This observation was quite surprising because normal levels of HDAC8 transcripts are generally lower than those of HDAC1 and HDAC3 in human cells, with the exception of some cancers, where HDAC8 expression is often strikingly upregulated.³⁵

The potential of smHDAC8 as a therapeutic target was supported by biochemical and in vivo assays.³⁶ RNA interference (RNAi)-mediated downregulation of smHDAC8 expression in schistosomula followed by their intravenous injection into mice and harvesting of the surviving worms 35 days later showed significantly reduced worm recovery compared with that from mice infected with schistosomula treated with control double-stranded RNA.³⁶ Finally, the crucial roles of zinc-dependent HDACs in schistosome biology were confirmed by the use of small-molecule HDAC inhibitors.^{33,36,37} Therefore, a therapy with small-molecule HDACi represents a promising approach for the treatment of schistosomiasis.

In a previous study, we were able to identify the first small-molecule inhibitors of smHDAC8 by a combination of virtual screening and in vitro testing.³⁸ Two of the identified hits were cocrystallized with smHDAC8, paving the way for structure-based optimization.³⁶ In the present work, we applied structure-based design on a benzohydroxamate template, taking into consideration appropriate synthetic strategies, to obtain compounds with smHDAC8 inhibitory activity in vitro and antischistosomal activity in cellular assays. A major goal of the current work was to identify compounds that show selectivity for smHDAC8 over major human HDAC isoforms, especially hHDAC1 and hHDAC6.

Scheme 1^a

^aConditions: (a) aldehyde, toluene, Na(AcO)₃BH, AcOH; (b) Boc₂O, MeOH, *t*-BuOH; (c) PyBOP, DIPEA, NH₂OTHP, THF; cat. HCl, THF; TFA, CHCl₃.

Scheme 2^a

^aConditions: (a) SOCl₂, MeOH; (b) DIPEA, THF; (c) aq. NaOH sol., MeOH; PyBOP, DIPEA, NH₂OTHP, THF; cat. HCl, THF.

RESULTS AND DISCUSSION

Structural Validation. From the available X-ray structure of smHDAC8/2³⁸ (Figure 1) it was known that a hydrogen bond is formed between the amide NH group of the inhibitor and His292.³⁸ Therefore, open-ring analogues that maintained this hydrogen bond were designed. This resulted in the synthesis of the first series of inhibitors, 3-aminobenzohydroxamates 10a–e (Scheme 1) and 3-amidobenzohydroxamates 13a–c (Scheme 2). In vitro testing showed that all compounds exhibit specificity for the HDAC8 isoforms over the other human HDACs tested (HDAC1 and -6). However, while the 3-aminobenzohydroxamates (10a–e) are micromolar inhibitors of both human and schistosomal HDAC8, they show a significant preference for the human isoform (Table 1). In contrast, the 3-amidobenzohydroxamates (13a–c) are active in the nanomolar range and show very similar inhibitory activities against hHDAC8 and smHDAC8. These results prompted us to focus on the derivatization of 13a–c, since this seemed to be a more promising strategy to obtain selective compounds.

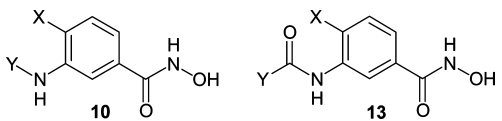
However, prior to the synthesis of derivatives of this series, we looked at the binding mode of this scaffold to smHDAC8. Toward this aim, the crystallographic structure of the complex between smHDAC8 and compound 13a at 2.2 Å was solved and refined (Table S1 in the Supporting Information). The crystal structure of the smHDAC8/13a complex reveals that the inhibitor binds in the smHDAC8 active-site pocket, forming specific interactions with the protein (Figure 2). First and as expected, the hydroxamate warhead of 13a interacts with the catalytic zinc ion and three residues, namely, His141, His142, and Tyr341 (Figure 2). The last of these residues adopts the flipped-in conformation typically observed in most HDAC/hydroxamate complexes.¹¹ Second, reminiscent of what was observed in the smHDAC8/2 complex,³⁶ smHDAC8 H292 is able to interact with inhibitor 13a, with its side chain forming a hydrogen bond (3.0 Å) with the amine group of the amide (Figures 2 and 3).

Strikingly, two additional smHDAC8-specific features were observed in this complex. First, and in contrast to what was observed for the smHDAC8/2 complex,³⁶ smHDAC8 Phe151 is observed to be in its flipped-out position (Figures 2 and 3) despite the fact that binding of 13a would not prevent the Phe151 side chain from adopting a flipped-in conformation. A major consequence of this flipped-out conformation of Phe151 is that Lys20 also adopts a flipped-in conformation, with the aliphatic part of its side chain lying on the Phe151 side chain and its amine forming a hydrogen bond (2.8 Å) with the carbonyl oxygen of the 13a amide group.

Interestingly, this is the first time that Lys20 has been observed to interact clearly with the inhibitor in an smHDAC8/inhibitor complex. Such a conformation had only been observed previously in the noninhibited structure of smHDAC8 in which Lys20 also interacted with an *L*-tartrate molecule that was present in the crystallization buffer and was observed to bind to the catalytic zinc (Figure 3). In all of the other smHDAC8/inhibitor complexes solved to date, the Lys20 side chain was either not seen in density or was prevented from reaching into the active site by the flipped-in conformation adopted by Phe151.³⁹

In addition to these hydrogen bonds formed between smHDAC8 and 13a, hydrophobic contacts between the two molecules are also observed, building on the overall hydrophobic character of the smHDAC8 active site and further stabilizing the smHDAC8/13a interaction. However, the schistosome-specific clamp formed by smHDAC8 Lys20 and His292, which distinctively interacts with the 13a amide group, helps anchor 13a in the enlarged (because Phe151 is flipped out) smHDAC8 active site, thus suggesting the molecular basis for the improved inhibitory activity of the 3-amidobenzohydroxamates toward smHDAC8.

Synthesis. We then continued the optimization of the 3-amidobenzohydroxamate inhibitors. Toward this aim and to guide the optimization process, docking studies using the

Table 1. IC₅₀ Values for 3-Aminobenzohydroxamate Derivatives


compound	X	Y	smHDAC8 IC ₅₀ (nM)	hHDAC8 IC ₅₀ (nM)	hHDAC1 IC ₅₀ (μM)	hHDAC6 IC ₅₀ (μM)
10a	H	benzyl	1080 ± 250	143.4 ± 7.3	41.4% @ 10 μM	n.d.
10b	H	cyclohexyl	3630 ± 620	830 ± 40	129.9 ± 18.5	n.d.
10c	H	N,N-dimethyl	1576 ± 146.0	70.2 ± 10.8	37.4% @ 10 μM	n.d.
10d	H	N,N-dibenzyl	9290 ± 1500	2190 ± 420	42.3 ± 3.8	8.6 ± 1.9
10e	methyl	cyclohexyl	600.3 ± 195.5	104.3 ± 12.0	49.5% @ 10 μM	n.d.
13a	H	phenyl	468.2 ± 79.0	582.0 ± 48.0	33.6 ± 1.8	3.0 ± 0.3
13b	methyl	phenyl	116.2 ± 38.2	204.0 ± 22.0	8.4 ± 2.0	0.9 ± 0.4
13c	methoxy	phenyl	189.8 ± 54.2	88.3 ± 24.0	2.3 ± 1.2	2.5 ± 1.1
13d	fluoro	phenyl	177.6 ± 8.1	317.8 ± 54.2	22.3 ± 7.7	0.50 ± 0.01
13e	chloro	phenyl	67.0 ± 10.2	120.0 ± 36.7	11.6 ± 3.9	0.12 ± 0.02
13f	bromo	phenyl	150.4 ± 8.5	191.4 ± 26.0	7.4 ± 0.8	0.15 ± 0.01
13g	trifluoromethyl	phenyl	139.6 ± 8.3	342.2 ± 76.1	2.4 ± 0.1	0.14 ± 0.02
13h	ethoxy	phenyl	129.3 ± 7.6	171.5 ± 15.6	4.6 ± 0.3	1.3 ± 0.1
13i	propoxy	phenyl	266.9 ± 49.5	n.d.	n.d.	n.d.
13j	isopropoxy	phenyl	220.1 ± 56.2	29.0 ± 0.2	3.6 ± 0.3	2.6 ± 0.4
13k	methyl	2-quinolinyl	96.1 ± 13.7	30.3 ± 7.3	2.7 ± 0.8	0.09 ± 0.01
13l	methoxy	4-biphenyl	75.4 ± 25.5	26.1 ± 17.6	6.3 ± 2.1	0.390 ± 0.002
13m	methoxy	4-methoxyphenyl	106.0 ± 17.5	77.1 ± 10.6	2.6 ± 0.2	0.4 ± 0.1
13n	methoxy	4-chlorophenyl	146.0 ± 4.3	239.7 ± 96.0	2.9 ± 0.3	0.9 ± 0.1
13o	methoxy	2-chlorophenyl	699.3 ± 27.4	211.16 ± 27.59	9.6 ± 1.0	3.1 ± 0.7
13p	methoxy	2,4-dichlorophenyl	121.6 ± 18.7	548.3 ± 93.9	13.0 ± 1.9	2.3 ± 0.4
13q	methoxy	3-biphenyl	289.7 ± 20.0	n.d.	n.d.	n.d.
13r	methoxy	4-ethoxyphenyl	305.0 ± 35.0	438.4 ± 48.0	4.4 ± 0.6	1.0 ± 0.1
13s	methoxy	benzyl	182.7 ± 39.3	512.2 ± 29.8	28.9 ± 8.6	5.1 ± 0.7
13t	chloro	4-methoxyphenyl	147.1 ± 4.8	235.6 ± 49.5	4.1 ± 0.9	0.13 ± 0.01
13u	chloro	3-benzyloxyphenyl	378.1 ± 44.9	214.4 ± 27.0	9.4 ± 2.8	1.5 ± 0.1
13v	chloro	3-phenoxyphenyl	396.4 ± 43.3	448.6 ± 100.4	6.4 ± 0.7	0.3 ± 0.1
13w	chloro	4-phenoxyphenyl	979.1 ± 1100	1080 ± 300	8.5 ± 2.1	0.15 ± 0.01
13x	chloro	4-chlorophenyl	234.7 ± 10.3	292.0 ± 53.3	3.8 ± 0.2	0.09 ± 0.05
13y	chloro	4-nitrophenyl	393.6 ± 50.5	n.d.	n.d.	n.d.
13z	chloro	2,4-dichlorophenyl	191.4 ± 16.7	1184.0 ± 45.1	31.6 ± 19.8	0.8 ± 0.1
13za	ethoxy	4-biphenyl	92.0 ± 26.0	148.7 ± 22.7	2.08 ± 0.14	0.6 ± 0.1
14a			8205 ± 1300	582.3 ± 88.5	n.d.	n.d.
15a			268.2 ± 21.1	23.9 ± 4.7	12.1 ± 5.7	2.9 ± 0.3
16a			485.0 ± 158.2	19.8 ± 5.9	20.0 ± 5.9	2.4 ± 0.9
17a			n.a.	n.a.	n.a.	n.a.
17b			n.a.	n.a.	n.a.	n.a.
1			1560 ± 200	400 ± 100	0.117 ± 0.006	0.042 ± 0.011
2			1480 ± 460	970 ± 110	27.5 ± 8.3	3.6 ± 0.6
3			1220 ± 280	620 ± 80	9.8 ± 0.7	1.3 ± 0.2
4			435.6 ± 61.0	77.7 ± 28.1	48% @ 100 μM	41% @ 100 μM

available inhibited hHDAC8 and smHDAC8 structures were carried out. Examination of the crystal structures showed that there is the possibility to use more bulky and more lipophilic residues at position 4 of the benzohydroxamate moiety. Recognizing that physicochemical properties might also play an important role in the antischistosomal activity, lipophilic substituents were also included. Taking this into consideration, we synthesized compounds **13d–j** containing different halides and alkoxy groups at position 4 to examine the effects of these substituents on the activity and selectivity for smHDAC8 (Scheme 2). The compounds containing halogen at position 4 of the benzohydroxamate moiety (**13d–f**) were slightly more selective for smHDAC8 compared with the 4-methoxy derivative **13c**. Compound **13h** with an ethoxy group at

position 4 did not show an increase in the activity against smHDAC8 but was less active on hHDAC8 compared with **13c**.

Meanwhile, analogues containing more lipophilic alkoxy residues at position 4, such as **13i** and **13j** (Scheme 2), exhibited decreased activity and selectivity for smHDAC8 compared with **13h**. Further modifications were introduced on the benzamide moiety, including chloro, nitro, and alkoxy groups (**13m–p**, **13r**, **13t**, **13x–z**). In addition, the introduction of aromatic lipophilic residues to address the hydrophobic side pocket of smHDAC8 (**13k**, **13l**, **13q**, **13u–w**, **13za**) was investigated. Compound **13k** bearing a quinolinyl residue and compound **13l** bearing a 4-biphenyl residue showed increased activity against smHDAC8 and hHDAC8.

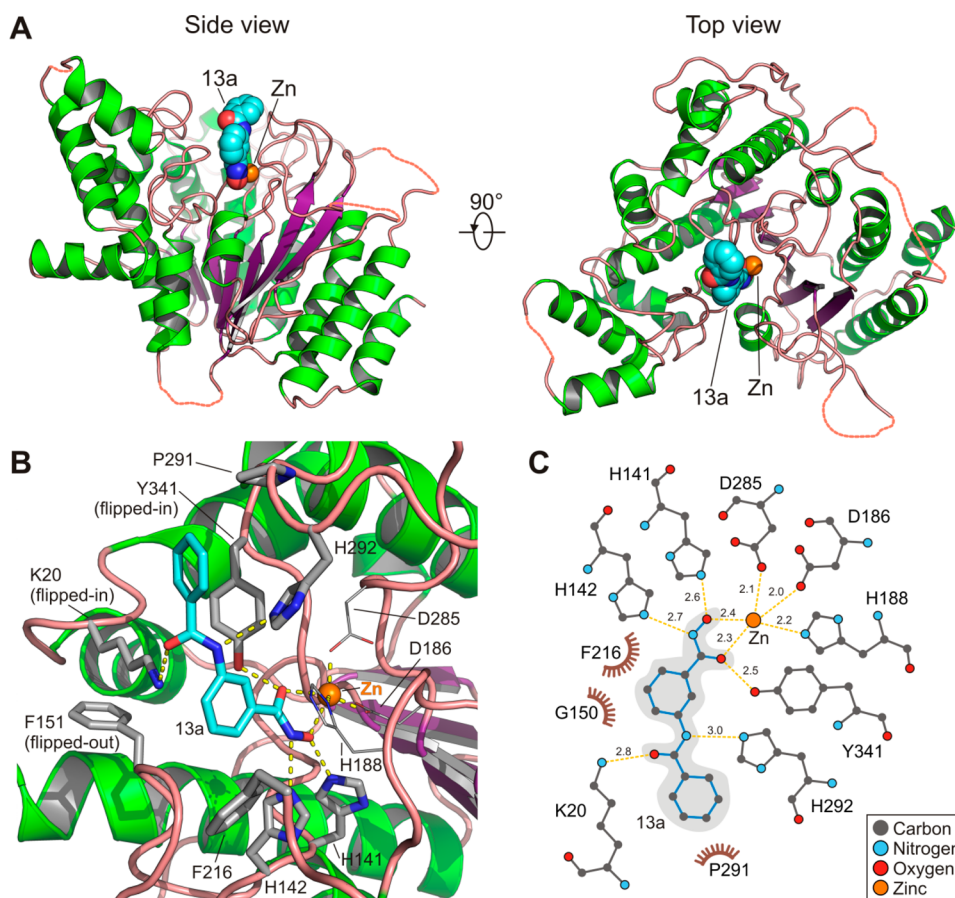


Figure 2. Overall structure of inhibitor **13a** bound to smHDAC8. (A) Structure of smHDAC8 (shown in ribbon representation) with bound **13a** (shown in space-filling representation). The orange sphere represents the catalytic zinc ion. (B) Close-up view of the binding mode of **13a** in the smHDAC8 active-site pocket. Protein residues are shown as gray sticks, and **13a** is shown as cyan sticks. Yellow dashed lines represent salt bridges made by smHDAC8, **13a**, and the catalytic zinc ion. (C) LigPlot-generated two-dimensional schematic overview of molecular interactions between **13a** and smHDAC8 active-site zinc and protein residues. Hydrogen bonds and interactions are indicated by yellow dashed lines, and the corresponding distances between the atoms (in Å) are given. Hydrophobic contacts are shown by brown arcs with spokes radiating toward the atoms involved.

Substitution at the meta position (as in **13q**) or the ortho position (as in **13o**) decreased the activity on the tested enzymes.

Interestingly, the combination of para and ortho substitution (as in **13p**) restored the activity against smHDAC8 without increasing the activity against the human enzymes. To prove that this substitution pattern is important for the selectivity of this compound, we synthesized compound **13z**, which was indeed found to be more active on the schistosomal enzyme than on the human counterpart. Increasing the distance between the two aromatic rings by a further methylene group (**13s**) led to increased smHDAC8 selectivity.

In addition, we tested other linker groups between the two aromatic rings (Scheme 3). The introduction of an ether (**15a**) or sulfonamide (**16a**) resulted in loss of activity for smHDAC8 and increased activity for hHDAC8 compared with **13c**. Also, using another scaffold such as a condensed aromatic ring system (**14a**) did not result in an improvement of the activity or selectivity compared with **13c**.

To check the impact of the zinc-chelating moiety, we synthesized two analogues of **13l** containing a carboxylate or carboxyl ester group instead of the hydroxamate (**17a** and **17b**, respectively; Scheme 4). As expected neither compound showed any effect in the enzymatic HDAC assay.

Docking Studies. To rationalize the obtained biochemical data, notably to understand the change in specificity between the schistosomal and human enzymes, the synthesized inhibitors were docked to the available crystal structures of smHDAC8, hHDAC8, and hHDAC1 and a homology model of hHDAC6. The applied docking method (for details, see Experimental Methods) was first successfully validated on the X-ray structures of hHDAC8 and smHDAC8. By means of this docking setup, consistent binding models were derived for both hHDAC8 and smHDAC8. In the case of smHDAC8, all of the derivatives having an amide linker between the two aromatic rings showed hydrogen bonds to Lys20 and His292, as observed for **13a** in its crystal structure.

Most importantly, the hydrogen bond between the amide linker and His292 cannot be formed in hHDAC8 since His292 is replaced by a methionine in this latter enzyme. However, in the available crystal structures of hHDAC8 a conserved water molecule bound to the zinc-coordinating histidine (His180 in hHDAC8) is observed, which was found to be a hydrogen-bonding partner with most of the amides in the docking studies (Figure 4). Thus, the observed hydrogen bond in the case of hHDAC8 (as well as in the homology model of HDAC6) could partially explain the same range of activity of some of the

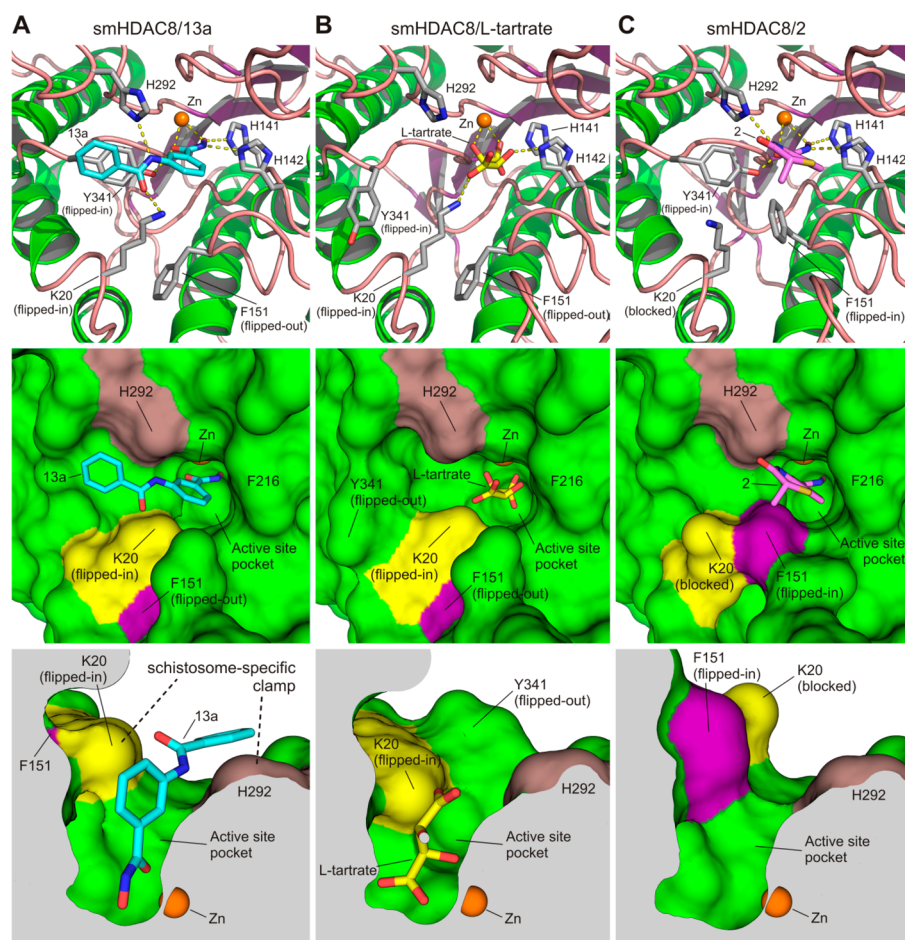
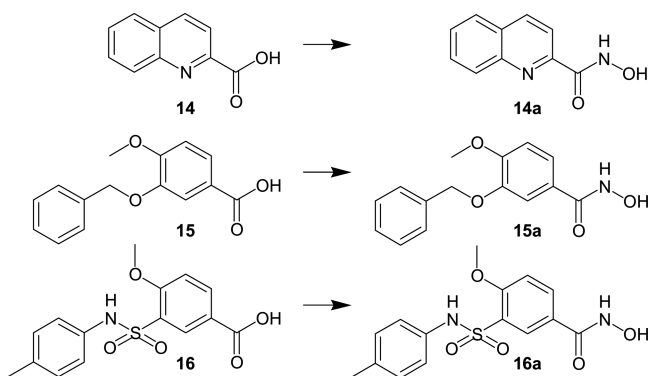


Figure 3. Specific structural interactions observed in the smHDAC8 active-site pocket in (A) the smHDAC8/13a complex, (B) the smHDAC8/*L*-tartrate complex, and (C) the smHDAC8/2 complex. Upper panels: close-up views with protein and small molecules shown as ribbon and sticks, respectively. Middle panels: surface representations. Lower panels: cutaway surface representations of the active site. For clarity, in (C) the 2 molecule was removed from the cutaway surface representation. In the smHDAC8/13a complex structure in (A), specific structural arrangements are observed, notably involving two specific residues: Lys20 and Phe151. The flipped-out conformation of Phe151 enables Lys20 to flip in and contact inhibitor 13a. This unique active-site conformation is not observed in other smHDAC8/inhibitor complexes. In addition, the schistosome-specific residue His292 together with the flipped-in Lys20 form a clamp that promotes stabilization and binding of 13a in the smHDAC8 active-site pocket.

Scheme 3^a



^aConditions: PyBOP, DIPEA, NH₂OTHP, THF; cat. HCl, THF.

compounds on the human HDAC8 and HDAC6 isoforms as on smHDAC8.

Adding a substituent at the para position of the parent compound 13a (methyl, alkyloxy, or halide) results in a 2- to 7-fold gain in smHDAC8 inhibitory potency and a 2- to 20-fold

gain in hHDAC8 potency (e.g., 13b, 13c, and 13e compared with 13a; Table 1). Increasing the size of the substituent at the para position enables additional interactions at the entrance of the pocket. Furthermore, the nature of the para substituent might influence the biologically active conformation of the compounds, which affects not only the potency but also the selectivity. In the case of compound 13a, the X-ray structure shows an out-of-plane orientation of the amide linker ($\Phi = -60^\circ$ to -102° ; Table S2 in the Supporting Information) that is stabilized by two hydrogen bonds to Lys20 and His292 (Figure 2). A substituent at the para position of the benzohydroxamate favors the out-of-plane conformation of the amide linker, which might explain the higher inhibitory potency of the para-substituted compounds. Measuring the dihedral angle Φ between the amide linker and the first aromatic ring observed in the docking poses shows a clear preference for the out-of-plane conformation of the amide group (-77° to -90° ; Table S2). In the case of hHDAC8, the predicted conformation of the amide linker is close to a coplanar orientation (29 – 51° , 148° for 13g) because of the modified hydrogen-bonding pattern (Figure 4).

Scheme 4

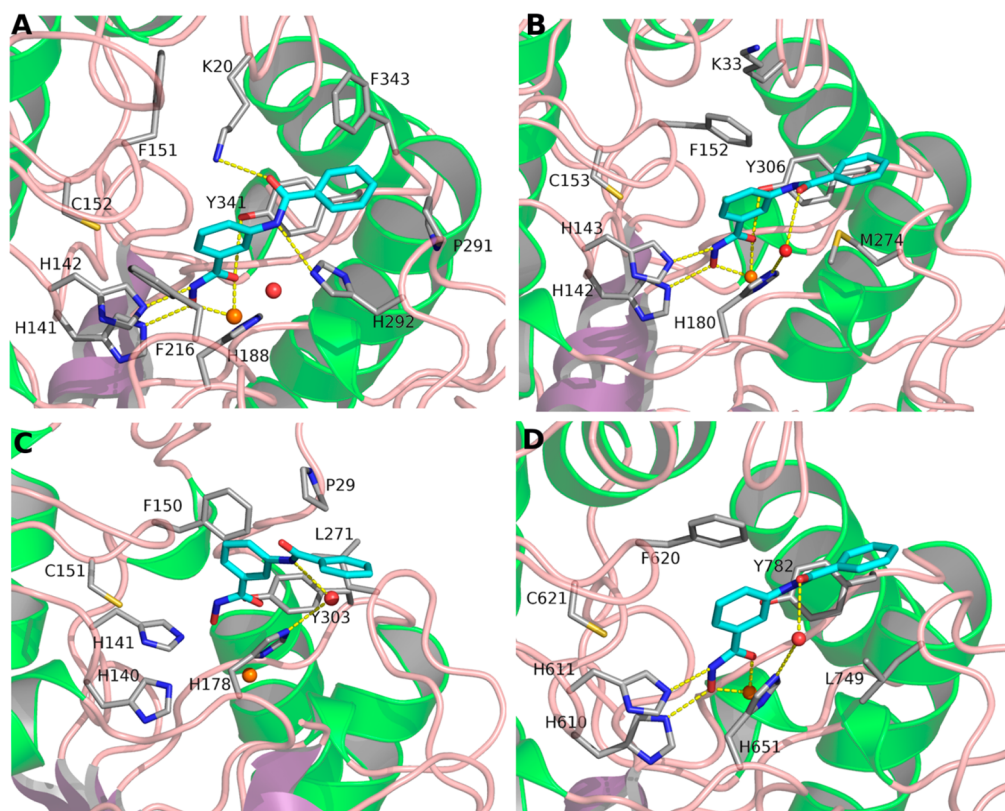
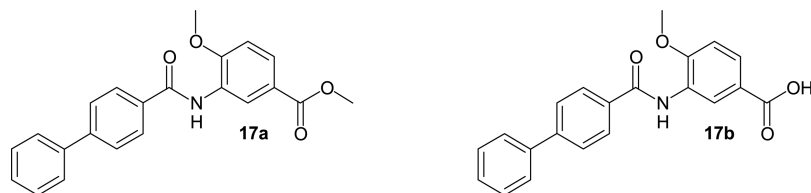


Figure 4. Docking poses of compound 13a (cyan carbon atoms) in (a–c) the X-ray structures of (a) smHDAC8 (this study), (b) hHDAC8 (PDB ID 2V5X), and (c) hHDAC1 (PDB ID SBKX) and (d) the homology model of hHDAC6. The protein backbone is depicted in ribbon representation, and the side chains of important residues are shown in stick representation with carbons colored gray. The conserved water molecule that should help stabilize the binding of 13a in the active sites of hHDAC6 and hHDAC8 is shown as a red ball, and the zinc ion is shown as an orange ball. Hydrogen bonds and interactions with the metal ion are depicted as yellow dashed lines.

The decreased HDAC1 activity might be attributed to the narrower pocket of hHDAC1 in comparison to hHDAC8 and -6. In the docking poses, this can be clearly seen in a comparison of the distances from the zinc-binding groups of meta-substituted benzohydroxamates to the zinc ion. In the case of hHDAC1, the distance is higher than in the other investigated HDAC isoforms (Figure 4). The docking results and structure–activity relationship studies suggest that meta substitution of benzohydroxamates is important to gain HDAC8 selectivity. This is also supported by previous publications showing that meta-substituted benzohydroxamic acids are more active on human HDAC8 and -6 in comparison with HDAC1 and other class I HDACs.^{28,30,40–45}

Adding hydrophobic substituents such as halides or further aromatic rings to the second aromatic ring (e.g., 13k, 13l, 13p, 13z, and 13za) resulted in additional van der Waals interactions with Phe216, Pro291, and Phe343 of smHDAC8. However, the higher selectivity of 13s and 13z (3–6-fold hHDAC8/smHDAC8 selectivity, 4–28-fold hHDAC6/smHDAC8 selectivity) could not be explained on the basis of the derived

docking solutions. More sophisticated methods that take into account protein flexibility and binding free energy calculations might be helpful to track down the subtle differences in the protein–ligand interactions deep inside the binding pocket.

Phenotypic Response. We next analyzed the effect of the developed compounds on the parasites maintained in culture. The compounds were initially tested for their toxicity toward *S. mansoni* schistosomula using an Alamar Blue-based viability assay (see Experimental Methods). Initial testing was done at a concentration of 10 μ M, and selected compounds were also tested at 20 μ M in order to determine the dose dependence. Two biological replicates were carried out in triplicate, and the results are shown in Table 2. In addition to the compounds developed during this study, the selective HDAC8 inhibitor 4 and praziquantel, the drug used for treatment of schistosomiasis, were also included in the assay. Of the tested compounds, 13l and 13za provoked the most marked dose-dependent reductions in schistosomula viability. In this assay, 4 showed only very modest activity against schistosomula, and praziquantel was inactive at the concentrations used. This latter

Table 2. Toxicity Studies on *S. mansoni* Schistosomula (Alamar Blue Assay)

compound	% viability \pm SEM	
	10 μ M	20 μ M
10b	82.7 \pm 2.4	n.d.
10c	92.6 \pm 7.4	n.d.
10d	77.9 \pm 2.6	74.6 \pm 0.4
10e	84.3 \pm 1.7	n.d.
13a	79.2 \pm 0.5	75.6 \pm 5.1
13b	82.9 \pm 2.0	72.4 \pm 2.4
13c	77.4 \pm 3.2	74.8 \pm 2.3
13d	82.0 \pm 8.1	78.6 \pm 9.5
13e	84.7 \pm 1.4	n.d.
13f	70.8 \pm 4.4	63.1 \pm 1.7
13g	99.9 \pm 0.8	77.4 \pm 3.4
13h	89.7 \pm 10.3	n.d.
13j	75.0 \pm 0.8	68.7 \pm 0.7
13k	74.9 \pm 4.1	59.4 \pm 4.2
13l	64.8 \pm 3.5	33.4 \pm 3.5
13m	74.6 \pm 6.7	64.6 \pm 1.0
13o	89.5 \pm 7.2	66.5 \pm 0.8
13p	77.8 \pm 2.4	50.7 \pm 2.7
13q	58.8 \pm 1.6	57.0 \pm 1.2
13s	83.3 \pm 4.2	82.8 \pm 5.8
13t	63.2 \pm 0.5	60.7 \pm 0.3
13u	73.8 \pm 5.4	68.6 \pm 2.4
13v	62.9 \pm 2.7	55.0 \pm 3.9
13x	71.8 \pm 4.1	49.3 \pm 0.6
13y	85.3 \pm 6.8	68.1 \pm 1.2
13z	72.5 \pm 0.3	59.3 \pm 9.9
13za	77.9 \pm 3.9	35.8 \pm 0.8
14a	95.6 \pm 4.4	n.d.
16a	77.7 \pm 5.0	73.8 \pm 4.2
4	70.6 \pm 0.5	62.3 \pm 3.5
praziquantel	92.0 \pm 7.5	89.0 \pm 5.7

result is in line with previous findings⁴⁶ and was thought to be due in part to the relatively weak activity of praziquantel on schistosomula and to stimulation of enzyme or ion channel activity, leading to high fluorescence signals in the assay. In view of its selectivity of inhibition with regard to human HDAC1 and -6, inhibitor **13l** was chosen for further testing. We first showed that the EC₅₀ value for this compound using the Alamar Blue-based assay was 16.1 μ M (Figure S1 in the Supporting Information). We next showed that compound **13l** is lethal to schistosomula in a microscopy-based assay within 2 days of incubation at 10 μ M and 1–2 days at 20 μ M (Figure 5A,B). We further tested **17a** and **17b** (Scheme 4), derivatives of **13l** that were synthesized as negative controls, to check **13l** for off-target effects. In the same assay, compound **17a**, an analogue of **13l** with a carboxyl ester instead of the hydroxamate that showed no inhibitory activity on smHDAC8, had only a very minor effect on schistosomula after 5 days of incubation compared with the dimethyl sulfoxide (DMSO) solvent control (Figure 5A,B). This suggested that the activity of **13l** on schistosomula is indeed related to its capacity to inhibit smHDAC8. We finally tested compound **13l** for its capacity to affect adult schistosomes maintained in culture (Figure 5C,D). At concentrations of 10 and 20 μ M, **13l** caused a marked separation of adult male and female worm pairs, with 90% of the pairs being separated after 5 days in the presence of 20 μ M **13l**. A corresponding reduction in egg laying by these

worm pairs was also induced (Figure 5D), reaching 80% for the 20 μ M dose. Therefore, compound **13l** affects the viability of both larvae and adult worms of *S. mansoni*, most probably through the inhibition of smHDAC8.

Cytotoxicity Assay. It was important to test the selectivity of the compounds against smHDAC8 and to exclude possible toxic effects caused by targeting of human HDACs or other proteins. Therefore, a cytotoxicity assay in a human epithelial kidney cell line (HEK293) was performed. The cells were incubated for 45 h with the indicated compounds at a concentration of 50 μ M, and the cell viability was determined using the Alamar Blue assay. All of the tested inhibitors exhibited only relatively low cytotoxicity in the human cell system used (Table 3).

CONCLUSIONS

Our initial work on HDAC8 from *Schistosoma mansoni* provided a proof of concept that HDAC inhibitors of this enzyme could be used to target pathogens.³⁶ Here a weak screening hit with suboptimal physicochemical properties characterized in that initial study was optimized against HDAC8 from *S. mansoni* using critical structure-guided insights. Central to this optimization was the inclusion of a methyl/methoxy group at the para position and an amide linker at the meta position of the benzohydroxamate. Previous crystallographic studies highlighted the binding of the inhibitors at the acetyllysine tunnel and featured a flexible phenylalanine that is able to shift in response to binding of compound to smHDAC8. The series disclosed here builds on this initial structural feature and represents a novel smHDAC8 inhibition template that provides the possibility to develop potent and selective inhibitors for the therapy of schistosomiasis. The presented compounds demonstrated high selectivity for smHDAC8 over the major human HDAC isoforms HDAC1 and -6, and some compounds even showed a preference for smHDAC8 over its human orthologue hHDAC8. It has been reported that inhibition of human HDAC8 shows limited effects on many cell types³⁹ and that an HDAC8 inhibitor had the most limited effect on the human acetylome among a panel of inhibitors of HDACs with different selectivities.⁴⁷ Cytotoxicity studies of the tested compounds showed that the compounds exhibit a relatively low effect on cell proliferation, indicating that the inhibition of human HDAC8 does not result in intrinsic toxicity. Thus, while we recognize that selectivity over human HDAC8 still needs optimization, there are strong indications that the high selectivity with respect to hHDAC1 and -6 that we have already obtained is more important for a potential therapeutic setting. The most potent derivatives were also shown to impair the viability of schistosomula without affecting cell viability of HEK293 cells. One such compound, **13l**, killed schistosomula in vitro and caused significant separation of adult worm pairs and a significant decrease in egg laying. An analogue of **13l** without inhibitory activity toward smHDAC8 had no effect on the parasite, confirming that inhibition of smHDAC8 is the basis of the antiparasitic effects of these inhibitors and underlining their potential as antischistosomal drug leads.

EXPERIMENTAL METHODS

Synthetic Chemistry. Unsubstituted and 4-substituted 3-amino-benzoic acids were used as starting points for the synthesis of the inhibitors under study. Alkyl and aryl residues were introduced on the aromatic NH₂ group via reductive amination of the imines obtained by

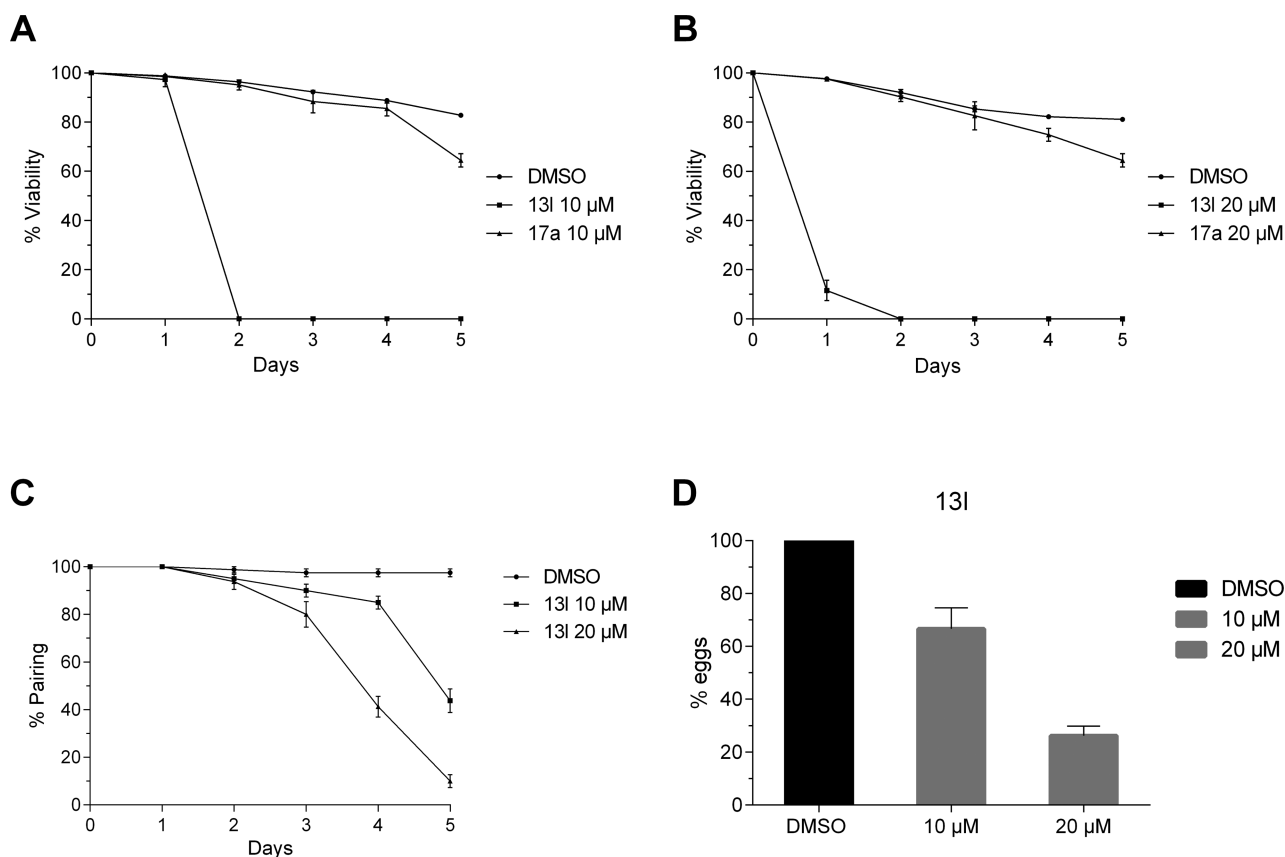


Figure 5. (A) Viability assay of *S. mansoni* schistosomula with up to 5 days of incubation with 10 μM 13l or 17a compared to the DMSO solvent control. (B) The same assay with 20 μM 13l or 17a. (C) Separation of adult worm pairs for up to 5 days in culture in the presence of 10 or 20 μM 13l. (D) Cumulative reduction (%) in egg laying by adult worm pairs in culture in the presence of 10 or 20 μM 13l compared with the DMSO solvent control.

Table 3. Cytotoxicity Studies in HEK293 Cells

compd	% viability ^a (%)	compd	% viability ^a (%)	compd	% viability ^a (%)
10a	n.d. ^b	13h	70.4	13t	62.5
10b	70.7	13i	97.4	13u	74.4
10c	92.7	13j	128.6	13v	62.0
10d	7.7	13k	66.2	13w	n.d.
10e	70.2	13l	12.3 (199 μM) ^c	13x	81.6
13a	72.0	13m	61.9	13y	79.1
13b	71.2	13n	92.6	13z	70.4
13c	67.3	13o	96.9	13za	80.3
13d	81.8	13p	95.1	14a	73.3
13e	72.2	13q	76.2	15a	69.1
13f	64.3	13r	87.7	16a	80.2
13g	96.0	13s	88.7	17a	47.2

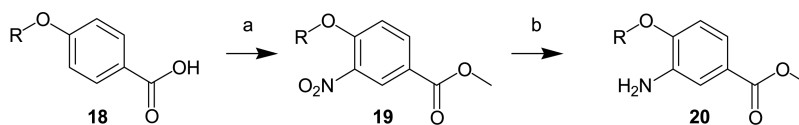
^aPercent viability of cells in the presence of 50 μM compound in comparison with an untreated sample. Daunorubicin was used as a positive control, and an IC_{50} value of $12.55 \pm 0.07 \mu\text{M}$ was determined. ^bn.d. = not determined. ^c IC_{50} value.

reaction of the amino group of the 3-aminobenzoic acids and an aldehyde using sodium triacetoxyborohydride as a reducing reagent. To avoid byproducts in the following synthetic steps, the secondary amine was protected by a *tert*-butyloxycarbonyl (Boc) group. The corresponding hydroxamates (10a–e) were obtained using PyBOP as an activating reagent and *O*-(tetrahydro-2*H*-pyran-2-yl)hydroxylamine and the subsequent cleavage of the protecting groups (Scheme 1). The 4-amidobenzohydroxamate derivatives 13a–g and 13k–z were prepared from different 3-aminobenzoic acids with modifications at

position 4 and various benzoic acid derivatives (14a–16a). The conversion of the amino group to the corresponding amide was accomplished by the reaction with activated benzoic acid derivatives and *N,N*-diisopropylethylamine (DIPEA). Different methods for activation of the carboxylic acids were tested. PyBOP, DCC, and chloroethyl formate were insufficient and formed byproducts, so activation with thionyl chloride was selected as the method of choice. Using methyl 3-aminobenzoate derivatives instead of 3-aminobenzoic acid derivatives increased the yields and also facilitated the purification. The corresponding hydroxamates were obtained using PyBOP and *O*-(tetrahydro-2*H*-pyran-2-yl)hydroxylamine followed by cleavage of the protecting group (Scheme 2). Generally, using tetrahydropyran (THP)-protected hydroxylamine increased the yields of the desired benzohydroxamates compared with other methods using hydroxylamine hydrochloride and KOH or potassium methanolate.

Several inhibitors (14a–16a) were synthesized directly from commercially available carboxylic acids (Scheme 3). In other cases (13h–j, 13za), the inhibitors were synthesized via compounds 20a–c, which were obtained starting from 4-alkoxybenzoic acids via a methyl esterification/nitration/reduction sequence (Scheme 5). For the nitration step, nitric acid, which is a mixture of 1 mL of nitric acid (68%) and 1.2 mL of sulfuric acid (98%), was used. This method is suitable for the reaction of 10 mmol of moderately activated aromatic rings. After the purification step, the nitro group was reduced to the corresponding amine group using Fe^0 and dilute hydrochloric acid.

Materials. All of the materials and reagents were purchased from Sigma-Aldrich Co. Ltd. and Carbolution Chemicals. All of the solvents were analytically pure and dried before use. Thin-layer chromatography was carried out on aluminum sheets coated with silica gel 60 F254 (Merck, Darmstadt, Germany). For column chromatography under normal pressure, silica gel 60 (0.036–0.200 mm) was used.

Scheme 5^a

R: **20a**) CH₃-CH₂-; **20b**) CH₃-(CH₂)₂-; **20c**) (CH₃)₂-CH-

^aConditions: (a) SOCl₂, MeOH, HNO₃/H₂SO₄; (b) Fe⁰, dil. HCl, MeOH.

Final compounds were confirmed to be of >95% purity based on HPLC. The purity was measured by UV absorbance at 256 nm. The HPLC system consisted of an XTerra RP18 column (3.5 μm 3.9 × 100 mm) from the manufacturer Waters (Milford, MA, USA), two LC-10AD pumps, an SPD-M10A VP PDA detector, and a SIL-HT autosampler, all from the manufacturer Shimadzu (Kyoto, Japan). The mobile phase was in all cases a gradient of methanol/water (starting at 95% water and going to 5% water).

Mass spectrometry analyses were performed with a Finnigan MAT 710C mass spectrometer (Thermo Separation Products, San Jose, CA, USA) for the ESI-MS spectra and with an LTQ (linear ion trap)-Orbitrap XL hybrid mass spectrometer (Thermo Fisher Scientific, Bremen, Germany) for the HRMS-ESI (high-resolution mass spectrometry) spectra. For the HRMS analyses, the signals for the isotopes with the highest prevalence (³⁵Cl, ⁷⁹Br) were given and calculated.

¹H and ¹³C NMR spectra were recorded on Varian Gemini 2000 and Varian Inova 500 spectrometers using deuterated chloroform (CDCl₃) and deuterated DMSO ((CD₃)₂SO) as solvents. Chemical shifts are referenced to the residual solvent signals. The following abbreviations for solvents and reagents were used: ethyl acetate (EtOAc), methanol (MeOH), tetrahydrofuran (THF), chloroform (CHCl₃), water (H₂O).

Computational Studies. Homology modeling of hHDAC6 was performed using the program MODELLER⁴⁸ as described in a previous publication.³⁸ Molecular docking of all of the inhibitors to the X-ray structures of smHDAC8, hHDAC8, and hHDAC1 and the homology model of hHDAC6 was carried out with the program Glide⁴⁹ (Schrödinger, LLC, New York, NY, USA) using the same protocol as in a previous study.³⁷ Briefly, the protein structures were prepared using Schrödinger's Protein Preparation Wizard. Hydrogen atoms were added, protonation states were assigned, and a restrained minimization was performed. Inhibitor structures were prepared in MOE 2012.10 (Chemical Computing Group, Montreal, Canada). All of the compounds were docked in neutral form with multiple low-energy starting conformations to produce more unbiased results.

Enzymes and in Vitro Inhibition Assays. Recombinant human HDAC1 and -6 were purchased from BPS Biosciences, and recombinant human HDAC8 was produced as described before.³⁶ Recombinant smHDAC8 enzyme was overproduced in *Escherichia coli* cells and purified by a method described previously.³⁶ Inhibition assays of smHDAC8 and human HDACs were performed as described earlier.^{36,37} Briefly, the commercial Fluor de Lys drug discovery kit (BML-KI178) was used to test the inhibition of smHDAC8 and human HDAC8. The test compound, Fluor de Lys-HDAC8 substrate (50 μM), and enzyme were incubated for 90 min at 37 °C with subsequent addition of 50 μL of Developer II (BML-KI176) and further incubation for 45 min at 30 °C. Fluorescence was measured in a plate reader (BMG Polarstar) with excitation at λ = 390 nm and emission at λ = 460 nm. Inhibition tests of human HDAC1 and -6 were conducted using Cbz-(Ac)Lys-AMC (ZMAL) as the substrate and trypsin as the developer. After incubation of the test compound, ZMAL (10.5 μM), and enzyme for 90 min at 37 °C, 60 μL of trypsin was added, and the mixture was further incubated for 20 min at 37 °C. Trichostatin A (2 μM) was used in both assays to stop the reaction. Fluorescence was measured as mentioned above. IC₅₀ values were determined with OriginPro version 9.0.0 (OriginLab, Northampton, MA, USA). Values in Table 1 represent mean ± standard error.

Cytotoxicity Studies. HEK293 cells (DSMZ Braunschweig, ACC305) were incubated at 37 °C in a humidified incubator with 5% CO₂ in Dulbecco's Modified Eagle's Medium (DMEM) supplemented with 10% fetal calf serum (FCS) and 5 mM glutamine. Cells were seeded out at 1.5 × 10³ cells per well in a 96-well cell-culture plate (TPP, Trasadingen, Switzerland). The test compound was added immediately to the medium at 50 μM or increasing concentrations to determine IC₅₀ values. After 24 h, Alamar Blue reagent (Invitrogen, CA) was added according to the manufacturer's instructions, and the mixture was incubated again for 21 h before samples were analyzed. Detection of viable cells, which convert the resazurine compound of the reagent into the highly fluorescent resorufin, was performed using a FLUOstar OPTIMA microplate reader (BMG Labtec, Ortenberg, Germany) with the following filter set: Ex 560 nm/Em 590 nm. All of the measurements were performed in triplicate, and the reported data are means with standard deviations of ≤12%. Daunorubicin was used as a positive control, and an IC₅₀ value of 12.55 ± 0.07 μM was determined.

Phenotypic Screening. The screening assay to determine the effects of novel inhibitors targeting smHDAC8 on the viability of *S. mansoni* schistosomula was carried out as previously described.⁵⁰ Briefly, newly transformed schistosomula (NTS) were obtained in vitro by mechanical transformation of *S. mansoni* cercaria as previously described.⁵¹ An NTS suspension was prepared at a concentration of 100 NTS per 100 μL using Medium 199 (Invitrogen) supplemented with 10% FCS (Gibco), penicillin (50 units mL⁻¹), streptomycin (50 μg mL⁻¹) and rifampicin (60 μg mL⁻¹). Schistosomula were kept in culture for 3 h at 37 °C and 5% CO₂ prior to use in screening. Drug stock solutions (20 mM in DMSO) were used. Mid-dilutions were performed in 100% DMSO, and 1 μL was added to 100 μL of M199 medium in the wells of black 96 well plates (Nunc, UK) supplemented with Medium 199 and 100 μL of prepared NTS suspension (100 NTS/well). Live and dead schistosomula (treated with 70% ethanol) were used as positive and negative controls. Experiments were carried out in triplicate wells in two biological replicates, and the compounds were tested at final concentrations of 10 and 20 μM. After 48 h of drug exposure, 20 μL of resazurine solution (AbdSerotec) was added to each well. Finally, after a further 24 h of exposure, the fluorescence intensity of the highly red-fluorescent resorufin product was measured at an excitation wavelength of 530 nm and an emission wavelength of 590 nm in an Infinite M200 Pro microplate reader (TECAN). Background fluorescence of the drug-containing medium was determined for each drug dilution using wells containing only DMSO as a control. The EC₅₀ for compound 13I was measured using the same assay with different concentrations of the compound.

The effect of selected compounds on the viability of schistosomula was further tested using a microscopy-based assay as described elsewhere.⁵² Schistosomula (2000 per well) prepared as described above were maintained in six-well plates in M199 medium kept at pH 7.4 with 10 mM HEPES and supplemented as above at 37 °C in a humid atmosphere containing 5% CO₂. Inhibitor (at 10 or 20 μM) was added, dissolved in DMSO, and the culture medium was refreshed each day. The assessment of parasite mortality was carried out after microscopic examination on the basis of three criteria: granular appearance, tegumental defects, and absence of motility. At least 300 schistosomula were observed at each time point for each condition, and the results were expressed as a percentage of viable larvae remaining. Three biological replicates (different batches of larvae) were examined in duplicate for each condition.

The stability of adult worm pairs and egg laying was assayed as previously described.⁵¹ Worm pairs were obtained from infected hamsters by perfusion as described previously⁵³ and washed in M199 medium, and 10 pairs were placed in 2 mL of M199 buffered complete medium (as for schistosomula above) in each well of a six-well culture plate. Worms were maintained in culture for 5 days at 37 °C (humid atmosphere, 5% CO₂) before the addition of smHDAC8 inhibitors dissolved in DMSO as above. Both the culture medium and the inhibitors were refreshed daily. The number of couples remaining as pairs was determined daily by microscopy, and the medium of each well containing eggs laid by the couples was recovered and centrifuged to allow the eggs to be counted under the microscope. Two biological replicate experiments were performed in triplicate.

Crystallization and X-ray Data Collection. Diffraction-quality crystals of native smHDAC8 enzyme were obtained at 17 °C after 3–4 days by mixing of equal volumes of smHDAC8 (2.5 mg/mL) with reservoir solution composed of 21% PEG 3350 (Fluka) and 0.2 M Na⁺/K⁺ L-tartrate and crystallization using the hanging-drop vapor diffusion technique. After 3 days, grown crystals were soaked in mother liquor supplemented with inhibitor 13a (10 mM final concentration of the inhibitor) for 20 h. Crystals used for X-ray data collection were briefly transferred in reservoir solution supplemented with 22% glycerol and flash-frozen in liquid nitrogen. Crystallographic data obtained in this project were collected at 100 K on SOLEIL beamline PROXIMA1.

Structure Determination, Model Building, and Refinement.

The crystallographic data were processed and scaled using HKL2000.⁵⁴ Since the crystals of the smHDAC8/13a complex belonged to the same space group (P1) and had the same unit cell as native smHDAC8 crystals,³⁶ only rigid-body refinement was used to adapt to the slight differences in unit cell constants using Phenix.⁵⁵ The initial model was refined through several cycles of manual building using Coot⁵⁶ and automated refinement with Phenix⁵⁵ and Buster.⁵⁷ The final model was validated using tools provided in Coot.⁵⁶ Visualization of structural data was done with Pymol,⁵⁸ and a two-dimensional diagram summarizing the molecular interactions between inhibitor 13a and smHDAC8 enzyme was prepared using the LigPlot program.⁵⁹ Atomic coordinates and structure factors of the smHDAC8/13a complex were deposited in the Protein Data Bank under PDB ID 5FUE.

■ ASSOCIATED CONTENT

📄 Supporting Information

The Supporting Information is available free of charge on the ACS Publications website at DOI: 10.1021/acs.jmedchem.5b01478.

X-ray data collection and refinement statistics for the smHDAC8/13a complex, dihedral angle analysis of docking poses of *m*-phenylamidobenzohydroxamates with different para substituents, Alamar Blue-based viability assay, and additional synthetic procedures and analytical data (PDF)

SMILES strings, IC₅₀ values, and percent viability data (CSV)

■ AUTHOR INFORMATION

Corresponding Author

*Phone: +493455525040. E-mail: wolfgang.sippl@pharmazie.uni-halle.de.

Author Contributions

[†]T.H. and A.C. contributed equally.

Notes

The authors declare no competing financial interest.

■ ACKNOWLEDGMENTS

This work and the authors of this article received funding from the European Union's Seventh Framework Programme for Research, Technological Development and Demonstration under Grant Agreements 241865 (SEtTReND) and 602080 (A-ParaDDisE). We thank Karin Schmidt-kunz, Simone Knies, Anja Kuberski, and Inka Negwer for technical assistance. The work of C.R. and M.M. was supported by institutional funds from the Centre National de la Recherche Scientifique (CNRS), the Institute National de la Santé et de la Recherche Médicale (INSERM), and the Université de Strasbourg. The work of J.L. and R.J.P. was supported by institutional funds from the CNRS, the Institut Pasteur de Lille, and the Université de Lille. This work was supported by the French Infrastructure for Integrated Structural Biology (FRISBI) ANR-10-INSB-05-01 and Instruct as part of the European Strategy Forum on Research Infrastructures (ESFRI). Work on human HDAC8 was supported by the Deutsche Forschungsgemeinschaft (Ju295/13-1 to M.J. and Si868/13-1 to W.S.). M.M., T.B.S., S.D., and C.R. thank members of SOLEIL for the use of their beamline facilities and for help during data collection.

■ ABBREVIATIONS USED

aq, aqueous; Boc, *tert*-butyloxycarbonyl; Boc₂O, di-*tert*-butyl dicarbonate; PyBOP, benzotriazol-1-yl-oxytripyridinophosphonium hexafluorophosphate; CDCl₃, deuterated chloroform; CEF, chloroethyl formate; CHCl₃, chloroform; DCC, dicyclohexylcarbodiimide; DIPEA, diisopropylethylamine; dDMSO, deuterated dimethyl sulfoxide; EtOAc, ethyl acetate; Et₃N, triethylamine; eq, equivalent; MeOH, methanol; Na(AcO)₃BH, sodium triacetoxyborohydride; n.a., not active; n.d., not determined; NH₂OTHP, *O*-(tetrahydro-2*H*-pyran-2-yl)-hydroxylamine; smHDAC8, *Schistosoma mansoni* histone deacetylase 8; SOCl₂, thionyl chloride; sol, solution; *t*-BuOH, *tert*-butyl alcohol; TEA, triethylamine; TFA, trifluoroacetic acid; THF, tetrahydrofuran; TLC, thin-layer chromatography

■ REFERENCES

- (1) Hotez, P. J.; Kamath, A. Neglected Tropical Diseases in Sub-Saharan Africa: Review of Their Prevalence, Distribution, and Disease Burden. *PLoS Neglected Trop. Dis.* **2009**, *3*, e412.
- (2) Brown, M. Schistosomiasis. *Clin. Med.* **2011**, *11*, 479–482.
- (3) Ross, A. G.; Bartley, P. B.; Sleigh, A. C.; Olds, G. R.; Li, Y.; Williams, G. M.; McManus, D. P. Schistosomiasis. *N. Engl. J. Med.* **2002**, *346*, 1212–1220.
- (4) Gray, D. J.; Ross, A. G.; Li, Y.-S.; McManus, D. P. Diagnosis and Management of Schistosomiasis. *BMJ.* **2011**, *342*, d2651.
- (5) World Health Organization. *Wkly. Epidemiol. Rec.* **2015**, *90*, 25–32.
- (6) Dömling, A.; Khoury, K. Praziquantel and Schistosomiasis. *ChemMedChem* **2010**, *5*, 1420–1421.
- (7) Ismail, M.; Botros, S.; Metwally, A.; William, S.; Farghally, A.; Tao, L.; Day, T. I. M. A.; Bennett, J. L. Resistance to Praziquantel: Direct Evidence from *Schistosoma mansoni* Isolated from Egyptian Villagers. *Am. J. Trop. Med. Hyg.* **1999**, *60*, 932–935.
- (8) Doenhoff, M. J.; Kusel, J. R.; Coles, G. C.; Cioli, D. Resistance of *Schistosoma mansoni* to Praziquantel: Is There a Problem? *Trans. R. Soc. Trop. Med. Hyg.* **2002**, *96*, 465–469.
- (9) Webster, J. P.; Molyneux, D. H.; Hotez, P. J.; Fenwick, A. The Contribution of Mass Drug Administration to Global Health: Past, Present and Future. *Philos. Trans. R. Soc., B* **2014**, *369*, 20130434.
- (10) Doenhoff, M. J.; Cioli, D.; Utzinger, J. Praziquantel: Mechanisms of Action, Resistance and New Derivatives for Schistosomiasis. *Curr. Opin. Infect. Dis.* **2008**, *21*, 659–667.

- (11) Marek, M.; Oliveira, G.; Pierce, R. J.; Jung, M.; Sippl, W.; Romier, C. Drugging the Schistosome Zinc-Dependent HDACs: Current Progress and Future Perspectives. *Future Med. Chem.* **2015**, *7*, 783–800.
- (12) Hotez, P. J.; Pecoul, B. Manifesto for Advancing the Control and Elimination of Neglected Tropical Diseases. *PLoS Neglected Trop. Dis.* **2010**, *4*, e718.
- (13) Schäfer, S.; Jung, M. Chromatin Modifications as Targets for New Anticancer Drugs. *Arch. Pharm.* **2005**, *338*, 347–357.
- (14) Pierce, R. J.; Dubois-Abdesselem, F.; Lancelot, J.; Andrade, L.; Oliveira, G. Targeting Schistosome Histone Modifying Enzymes for Drug Development. *Curr. Pharm. Des.* **2012**, *18*, 3567–3578.
- (15) Andrews, K. T.; Haque, A.; Jones, M. K. HDAC Inhibitors in Parasitic Diseases. *Immunol. Cell Biol.* **2012**, *90*, 66–77.
- (16) Ouaisi, M.; Ouaisi, A. Histone Deacetylase Enzymes as Potential Drug Targets in Cancer and Parasitic Diseases. *J. Biomed. Biotechnol.* **2006**, *2006*, 13474.
- (17) Grunstein, M. Histone Acetylation in Chromatin Structure and Transcription. *Nature* **1997**, *389*, 349–352.
- (18) Peserico, A.; Simone, C. Physical and Functional HAT/HDAC Interplay Regulates Protein Acetylation Balance. *J. Biomed. Biotechnol.* **2011**, *2011*, 371832.
- (19) Yang, X. J.; Seto, E. The Rpd3/Hda1 Family of Lysine Deacetylases: From Bacteria and Yeast to Mice and Men. *Nat. Rev. Mol. Cell Biol.* **2008**, *9*, 206–218.
- (20) North, B. J.; Verdin, E. Sirtuins: Sir2-Related NAD-Dependent Protein Deacetylases. *Genome Biol.* **2004**, *5*, 224.
- (21) Cho, Y. S.; Whitehead, L.; Li, J.; Chen, C. H. T.; Jiang, L.; Vögtle, M.; Francotte, E.; Richert, P.; Wagner, T.; Traebert, M.; Lu, Q.; Cao, X.; Dumotier, B.; Fejzo, J.; Rajan, S.; Wang, P.; Yan-Neale, Y.; Shao, W.; Atadja, P.; Shultz, M. Conformational Refinement of Hydroxamate-Based Histone Deacetylase Inhibitors and Exploration of 3-Piperidin-3-Ylindole Analogues of Dacinostat (LAQ824). *J. Med. Chem.* **2010**, *53*, 2952–2963.
- (22) Marks, P.; Rifkind, R. A.; Richon, V. M.; Breslow, R.; Miller, T.; Kelly, W. K. Histone Deacetylases and Cancer: Causes and Therapies. *Nat. Rev. Cancer* **2001**, *1*, 194–202.
- (23) Ito, K.; Ito, M.; Elliott, W. M.; Cosio, B.; Caramori, G.; Kon, O. M.; Barczyk, A.; Hayashi, S.; Adcock, I. M.; Hogg, J. C.; Barnes, P. J. Decreased Histone Deacetylase Activity in Chronic Obstructive Pulmonary Disease. *N. Engl. J. Med.* **2005**, *352*, 1967–1976.
- (24) Mukherjee, P.; Pradhan, A.; Shah, F.; Tekwani, B. L.; Avery, M. A. Structural Insights into the Plasmodium Falciparum Histone Deacetylase 1 (PfHDAC-1): A Novel Target for the Development of Antimalarial Therapy. *Bioorg. Med. Chem.* **2008**, *16*, 5254–5265.
- (25) Giannini, G.; Cabri, W.; Fattorusso, C.; Rodriguez, M. Histone Deacetylase Inhibitors in the Treatment of Cancer: Overview and Perspectives. *Future Med. Chem.* **2012**, *4*, 1439–1460.
- (26) Marks, P. A.; Breslow, R. Dimethyl sulfoxide to vorinostat: development of this histone deacetylase inhibitor as an anticancer drug. *Nat. Biotechnol.* **2007**, *25*, 84–90.
- (27) Balasubramanian, S.; Ramos, J.; Luo, W.; Sirisawad, M.; Verner, E.; Buggy, J. J. A novel histone deacetylase 8 (HDAC8)-specific inhibitor PCI-34051 induces apoptosis in T-cell lymphomas. *Leukemia* **2008**, *22*, 1026–1034.
- (28) Suzuki, T.; Ota, Y.; Ri, M.; Bando, M.; Gotoh, A.; Itoh, Y.; Tsumoto, H.; Tatum, P. R.; Mizukami, T.; Nakagawa, H.; Iida, S.; Ueda, R.; Shirahige, K.; Miyata, N. Rapid Discovery of Highly Potent and Selective Inhibitors of Histone Deacetylase 8 Using Click Chemistry to Generate Candidate Libraries. *J. Med. Chem.* **2012**, *55*, 9562–9575.
- (29) Huang, W. J.; Wang, Y. C.; Chao, S. W.; Yang, C. J.; Chen, L. C.; Lin, M. H.; Hou, W. C.; Chen, M. Y.; Lee, T. L.; Yang, P.; Chang, C. I. Synthesis and biological evaluation of ortho-aryl N-hydroxycinnamides as potent histone deacetylase (HDAC) 8 isoform-selective inhibitors. *ChemMedChem* **2012**, *7*, 1815–1824.
- (30) Suzuki, T.; Muto, N.; Bando, M.; Itoh, Y.; Masaki, A.; Ri, M.; Ota, Y.; Nakagawa, H.; Iida, S.; Shirahige, K.; Miyata, N. Design, synthesis, and biological activity of NCC149 derivatives as histone deacetylase 8-selective inhibitors. *ChemMedChem* **2014**, *9*, 657–664.
- (31) Andrews, K. T.; Walduck, A.; Kelso, M. J.; Fairlie, D. P.; Saul, A.; Parsons, P. G. Anti-Malarial Effect of Histone Deacetylation Inhibitors and Mammalian Tumour Cytodifferentiating Agents. *Int. J. Parasitol.* **2000**, *30*, 761–768.
- (32) Oger, F.; Dubois, F.; Caby, S.; Noël, C.; Cornette, J.; Bertin, B.; Capron, M.; Pierce, R. J. The Class I Histone Deacetylases of the Platyhelminth Parasite *Schistosoma mansoni*. *Biochem. Biophys. Res. Commun.* **2008**, *377*, 1079–1084.
- (33) Dubois, F.; Caby, S.; Oger, F.; Cosseau, C.; Capron, M.; Grunau, C.; Dissous, C.; Pierce, R. J. Histone Deacetylase Inhibitors Induce Apoptosis, Histone Hyperacetylation and up-Regulation of Gene Transcription in *Schistosoma mansoni*. *Mol. Biochem. Parasitol.* **2009**, *168*, 7–15.
- (34) Lancelot, J.; Caby, S.; Dubois-Abdesselem, F.; Vanderstraete, M.; Trolet, J.; Oliveira, G.; Bracher, F.; Jung, M.; Pierce, R. J. *Schistosoma mansoni* sirtuins: characterization and potential as chemotherapeutic targets. *PLoS Neglected Trop. Dis.* **2013**, *7*, e2428.
- (35) Nakagawa, M.; Oda, Y.; Eguchi, T.; Aishima, S.-I.; Yao, T.; Hosoi, F.; Basaki, Y.; Ono, M.; Kuwano, M.; Tanaka, M.; Tsuneyoshi, M. Expression Profile of Class I Histone Deacetylases in Human Cancer Tissues. *Oncol. Rep.* **2007**, *18*, 769–774.
- (36) Marek, M.; Kannan, S.; Hauser, A. T.; Moraes Mourão, M.; Caby, S.; Cura, V.; Stolfa, D. A.; Schmidtkunz, K.; Lancelot, J.; Andrade, L.; Renaud, J. P.; Oliveira, G.; Sippl, W.; Jung, M.; Cavarelli, J.; Pierce, R. J.; Romier, C. Structural Basis for the Inhibition of Histone Deacetylase 8 (HDAC8), a Key Epigenetic Player in the Blood Fluke *Schistosoma mansoni*. *PLoS Pathog.* **2013**, *9*, e1003645.
- (37) Stolfa, D.; Marek, M.; Lancelot, J.; Hauser, A.-T.; Walter, A.; Leproult, E.; Melesina, J.; Rumpf, T.; Wurtz, J.-M.; Cavarelli, J.; Sippl, W.; Pierce, R. J.; Romier, C.; Jung, M. Molecular Basis for the Antiparasitic Activity of a Mercaptoacetamide Derivative That Inhibits Histone Deacetylase 8 (HDAC8) from the Human Pathogen *Schistosoma mansoni*. *J. Mol. Biol.* **2014**, *426*, 3442–3453.
- (38) Kannan, S.; Melesina, J.; Hauser, A.; Chakrabarti, A.; Heimburg, T.; Schmidtkunz, K.; Walter, A.; Marek, M.; Pierce, R. J.; Romier, C.; Jung, M.; Sippl, W. Discovery of Inhibitors of *Schistosoma mansoni* HDAC8 by Combining Homology Modeling, Virtual Screening, and in Vitro Validation. *J. Chem. Inf. Model.* **2014**, *54*, 3005–3019.
- (39) Chakrabarti, A.; Oehme, I.; Witt, O.; Oliveira, G.; Sippl, W.; Romier, C.; Pierce, R. J.; Jung, M. HDAC8: A Multifaceted Target for Therapeutic Interventions. *Trends Pharmacol. Sci.* **2015**, *36*, 481–92.
- (40) Rodrigues, D. A.; Ferreira-Silva, G. Á.; Ferreira, A. C. S.; Fernandes, R. A.; Kwee, J. K.; Sant’Anna, C. M. R.; Ionta, M.; Fraga, C. A. M. Design, Synthesis, and Pharmacological Evaluation of Novel N-Acylhydrazono Derivatives as Potent Histone Deacetylase 6/8 Dual Inhibitors. *J. Med. Chem.* **2016**, *59*, 655–670.
- (41) Wang, L.; Kofler, M.; Brosch, G.; Melesina, J.; Sippl, W.; Martinez, E. D.; Easmon, J. 2-Benzazoyl-4-Piperazin-1-Ylsulfonylbenzenecarbo-hydroxamic Acids as Novel Selective Histone Deacetylase-6 Inhibitors with Antiproliferative Activity. *PLoS One* **2015**, *10*, e0134556.
- (42) Lobera, M.; Madauss, K. P.; Pohlhaus, D. T.; Wright, Q. G.; Trocha, M.; Schmidt, D. R.; Baloglu, E.; Trump, R. P.; Head, M. S.; Hofmann, G. A.; Murray-Thompson, M.; Schwartz, B.; Chakravorty, S.; Wu, Z.; Mander, P. K.; Kruidenier, L.; Reid, R. A.; Burkhart, W.; Turunen, B. J.; Rong, J. X.; Wagner, C.; Moyer, M. B.; Wells, C.; Hong, X.; Moore, J. T.; Williams, J. D.; Soler, D.; Ghosh, S.; Nolan, M. A. Selective class IIa histone deacetylase inhibition via a nonchelating zinc-binding group. *Nat. Chem. Biol.* **2013**, *9*, 319–325.
- (43) Olson, D. E.; Wagner, F. F.; Kaya, T.; Gale, J. P.; Aidoud, N.; Davoine, E. L.; Lazzaro, F.; Weiwler, M.; Zhang, Y. L.; Holson, E. B. Discovery of the First Histone Deacetylase 6/8 Dual Inhibitors. *J. Med. Chem.* **2013**, *56*, 4816–4820.
- (44) Tang, W.; Luo, T.; Greenberg, E. F.; Bradner, J. E.; Schreiber, S. L. Discovery of histone deacetylase 8 selective inhibitors. *Bioorg. Med. Chem. Lett.* **2011**, *21*, 2601–2605.

(45) KrennHrubec, K.; Marshall, B. L.; Hedglin, M.; Verdin, E.; Ulrich, S. Ma. Design and evaluation of 'Linkerless' hydroxamic acids as selective HDAC8 inhibitors. *Bioorg. Med. Chem. Lett.* **2007**, *17*, 2874–2878.

(46) Panic, G.; Flores, D.; Ingram-Sieber, K.; Keiser, J. Fluorescence/luminescence-based markers for the assessment of *Schistosoma mansoni* schistosomula drug assays. *Parasites Vectors* **2015**, *8*, 624.

(47) Choudhary, C.; Kumar, C.; Gnad, F.; Nielsen, M. L.; Rehman, M.; Walther, T. C.; Olsen, J. V.; Mann, M. Lysine Acetylation Targets Protein Complexes and Co-Regulates Major Cellular Functions. *Science* **2009**, *325*, 834–840.

(48) Eswar, N.; Webb, B.; Marti-Renom, M. A.; Madhusudhan, M. S.; Eramian, D.; Shen, M. Y.; Pieper, U.; Sali, A. Comparative Protein Structure Modeling Using Modeller. *Current Protocols in Bioinformatics*; Wiley: New York, **2006**; Chapter 5, Unit 5.6.

(49) Suite 2012: Maestro Version 9.3, Protein Preparation Wizard, Epik Version 2.3, Glide Version 5.8; Schrödinger, LLC: New York, 2012.

(50) Marxer, M.; Ingram, K.; Keiser, J. Development of an in Vitro Drug Screening Assay Using *Schistosoma haematobium* schistosomula. *Parasites Vectors* **2012**, *5*, 165.

(51) Ramalho-Pinto, F. J.; Gazzinelli, G.; Howells, R. E.; Mota-Santos, T.; Figueiredo, E.; Pellegrino, J. *Schistosoma mansoni*: Defined System for Stepwise Transformation of Cercaria to Schistosomule in Vitro. *Exp. Parasitol.* **1974**, *36*, 360–372.

(52) Vanderstraete, M.; Gouignard, N.; Cailliau, K.; Morel, M.; Lancelot, J.; Bodart, J. F.; Dissous, C. Dual Targeting of Insulin and Venus Kinase Receptors of *Schistosoma mansoni* for Novel Anti-Schistosome Therapy. *PLoS Neglected Trop. Dis.* **2013**, *7*, e2226.

(53) Smithers, S. R.; Terry, R. J. The Infection of Laboratory Hosts with Cercariae of *Schistosoma mansoni* and the Recovery of the Adult Worms. *Parasitology* **1965**, *55*, 695–700.

(54) Otwinowski, Z.; Minor, W. Processing of X-ray diffraction data collected in oscillation mode. *Methods Enzymol.* **1997**, *276*, 307–326.

(55) Adams, P. D.; Afonine, P. V.; Bunkóczi, G.; Chen, V. B.; Davis, I. W.; Echols, N.; Headd, J. J.; Hung, L.-W.; Kapral, G. J.; Grosse-Kunstleve, R. W.; McCoy, A. J.; Moriarty, N. W.; Oeffner, R.; Read, R. J.; Richardson, D. C.; Richardson, J. S.; Terwilliger, T. C.; Zwart, P. H. PHENIX: A comprehensive Python-based system for macromolecular structure solution. *Acta Crystallogr., Sect. D: Biol. Crystallogr.* **2010**, *66*, 213–221.

(56) Emsley, P.; Cowtan, K. Coot: model-building tools for molecular graphics. *Acta Crystallogr., Sect. D: Biol. Crystallogr.* **2004**, *60*, 2126–2132.

(57) Blanc, E.; Roversi, P.; Vonrhein, C.; Flensburg, C.; Lea, S. M.; Bricogne, G. Refinement of severely incomplete structures with maximum likelihood in BUSTER-TNT. *Acta Crystallogr., Sect. D: Biol. Crystallogr.* **2004**, *60*, 2210–2221.

(58) The PyMOL Molecular Graphics System, version 1.7.4; Schrödinger, LLC: New York.

(59) Wallace, A. C.; Laskowski, R. A.; Thornton, J. M. LIGPLOT: a program to generate schematic diagrams of protein-ligand interactions. *Protein Eng., Des. Sel.* **1995**, *8*, 127–134.